

Beam steering for virtual/augmented reality displays with a cycloidal diffractive waveplate

Haiwei Chen,¹ Yishi Weng,^{1,2} Daming Xu,¹ Nelson V. Tabiryan,³ and Shin-Tson Wu^{1,*}

¹College of Optics and Photonics, University of Central Florida, Orlando, Florida 32816, USA

²School of Electronic Science and Engineering, Southeast University, Nanjing 210018, China

³Beam Engineering for Advanced Measurements Co., Orlando, Florida 32810, USA

*swu@ucf.edu

Abstract: We proposed a switchable beam steering device with cycloidal diffractive waveplate (CDW) for eye tracking in a virtual reality (VR) or augmented reality (AR) display system. Such a CDW diffracts the incident circularly polarized light to the first order with over 95% efficiency. To convert the input linearly polarized light to right-handed or left-handed circular polarization, we developed a broadband polarization switch consisting of a twisted nematic liquid crystal cell and an achromatic quarter-wave retardation film. By cascading 2-3 CDWs together, multiple diffraction angles can be achieved. To suppress the color dispersion, we proposed two approaches to obtain the same diffraction angle for red, green, and blue LEDs-based full color displays. Our device exhibits several advantages, such as high diffraction efficiency, fast response time, low power consumption, and low cost. It holds promise for the emerging VR/AR displays.

©2016 Optical Society of America

OCIS codes: (050.1950) Diffraction gratings; (160.3710) Liquid crystals; (230.2090) Electro-optical devices.

References and links

1. O. Cakmakci and J. Rolland, "Head-worn displays: a review," *J. Disp. Technol.* **2**(3), 199–216 (2006).
2. B. Furht, *Handbook of Augmented Reality* (Springer, 2011).
3. R. A. Earnshaw, *Virtual Reality Systems* (Academic, 2014).
4. K. Akeley, S. J. Watt, A. R. Girshick, and M. S. Banks, "A stereo display prototype with multiple focal distances," *ACM Trans. Graph.* **23**(3), 804–813 (2004).
5. V. Tanriverdi and R. J. Jacob, "Interacting with eye movements in virtual environments," *Chin. Lett.* **2**(1), 265–272 (2000).
6. A. T. Duchowski, V. Shivashankaraiyah, T. Rawls, A. K. Gramopadhye, B. J. Melloy, and B. Kanki, "Binocular eye tracking in virtual reality for inspection training," in *Proceedings of the 2000 Symposium on Eye Tracking Research and Applications* (ACM, 2000), pp. 89–96.
7. F. Zhou, H. B. L. Duh, and M. Billinghurst, "Trends in augmented reality tracking, interaction and display: A review of ten years of ISMAR," in *Proceedings of the 7th IEEE/ACM International Symposium on Mixed and Augmented Reality* (ACM, 2008) pp. 193–202.
8. N. C. Tien, O. Solgaard, M. H. Kiang, M. Daneman, K. Y. Lau, and R. S. Muller, "Surface-micromachined mirrors for laser-beam positioning," *Sens. Actuators A Phys.* **52**(1), 76–80 (1996).
9. N. R. Smith, D. C. Abeysinghe, J. W. Haus, and J. Heikenfeld, "Agile wide-angle beam steering with electrowetting microprisms," *Opt. Express* **14**(14), 6557–6563 (2006).
10. P. F. McManamon, P. J. Bos, M. J. Escuti, J. Heikenfeld, S. Serati, H. Xie, and E. A. Watson, "A review of phased array steering for narrow-band electrooptical systems," *Proc. IEEE* **97**(6), 1078–1096 (2009).
11. S. R. Davis, G. Farca, S. D. Rommel, S. Johnson, and M. H. Anderson, "Liquid crystal waveguides: new devices enabled by > 1000 waves of optical phase control," *Proc. SPIE* **7618**, 76180E (2010).
12. C. Provenzano, P. Pagliusi, and G. Cipparrone, "Highly efficient liquid crystal based diffraction grating induced by polarization holograms at the aligning surfaces," *Appl. Phys. Lett.* **89**(12), 121105 (2006).
13. S. Serak, N. Tabiryan, and B. Zeldovich, "High-efficiency 1.5 μm thick optical axis grating and its use for laser beam combining," *Opt. Lett.* **32**(2), 169–171 (2007).
14. C. Oh and M. J. Escuti, "Achromatic diffraction from polarization gratings with high efficiency," *Opt. Lett.* **33**(20), 2287–2289 (2008).

15. S. R. Nersisyan, N. V. Tabiryan, D. M. Steeves, and B. R. Kimball, "Optical axis gratings in liquid crystals and their use for polarization insensitive optical switching," *J. Nonlinear Opt. Phys. Mater.* **18**(1), 1–47 (2009).
16. N. V. Tabiryan, S. R. Nersisyan, D. M. Steeves, and B. R. Kimball, "The promise of diffractive waveplates," *Opt. Photonics News* **21**, 41–45 (2010).
17. H. Sarkissian, S. V. Serak, N. V. Tabiryan, L. B. Glebov, V. Rotar, and B. Y. Zeldovich, "Polarization-controlled switching between diffraction orders in transverse-periodically aligned nematic liquid crystals," *Opt. Lett.* **31**(15), 2248–2250 (2006).
18. S. R. Nersisyan, N. V. Tabiryan, D. M. Steeves, and B. R. Kimball, "The principles of laser beam control with polarization gratings introduced as diffractive waveplates," *Proc. SPIE* **7775**, 77750U (2010).
19. S. R. Nersisyan, N. V. Tabiryan, L. Hoke, D. M. Steeves, and B. R. Kimball, "Polarization insensitive imaging through polarization gratings," *Opt. Express* **17**(3), 1817–1830 (2009).
20. S. T. Wu, U. Efron, and L. D. Hess, "Birefringence measurements of liquid crystals," *Appl. Opt.* **23**(21), 3911–3915 (1984).
21. M. Schadt and W. Helfrich, "Voltage-dependent optical activity of a twisted nematic liquid crystal," *Appl. Phys. Lett.* **18**(4), 127–128 (1971).
22. H. Ren, S. Xu, Y. Liu, and S. T. Wu, "Switchable focus using a polymeric lenticular microlens array and a polarization rotator," *Opt. Express* **21**(7), 7916–7925 (2013).
23. R. Zhu, S. Xu, Q. Hong, S. T. Wu, C. Lee, C. M. Yang, C. C. Lo, and A. Lien, "Polymeric-lens-embedded 2D/3D switchable display with dramatically reduced crosstalk," *Appl. Opt.* **53**(7), 1388–1395 (2014).
24. S. Gauza, X. Zhu, W. Piecek, R. Dabrowski, and S. T. Wu, "Fast switching liquid crystals for color-sequential LCDs," *J. Disp. Technol.* **3**(3), 250–252 (2007).
25. H. Chen, F. Peng, Z. Luo, D. Xu, S. T. Wu, M. C. Li, S. L. Lee, and W. C. Tsai, "High performance liquid crystal displays with a low dielectric constant material," *Opt. Mater. Express* **4**(11), 2262–2273 (2014).
26. H. Chen, M. Hu, F. Peng, J. Li, Z. An, and S. T. Wu, "Ultra-low viscosity liquid crystals," *Opt. Mater. Express* **5**(3), 655–660 (2015).
27. S. T. Wu and C. S. Wu, "High-speed liquid-crystal modulators using transient nematic effect," *J. Appl. Phys.* **65**(2), 527–532 (1989).
28. S. T. Wu, "Nematic liquid crystal modulator with response time less than 100 μ s at room temperature," *Appl. Phys. Lett.* **57**(10), 986–988 (1990).
29. A. Chao, K. T. Huang, C. W. Tsai, Y. W. Hung, H. F. Cheng, W. Yeh, C. H. Yu, and H. H. Wu, "The fastest response TN-Type TFT LCD of the world likes OCB level," *SID Int. Symp. Digest Tech. Papers* **38**(1), 603–606 (2007).
30. H. Xianyu, S. T. Wu, and C. L. Lin, "Dual frequency liquid crystals: a review," *Liq. Cryst.* **36**(6–7), 717–726 (2009).
31. K. Holmqvist, M. Nyström, R. Andersson, R. Dewhurst, H. Jarodzka, and J. Van de Weijer, *Eye Tracking: A Comprehensive Guide to Methods and Measures* (Oxford University, 2011).
32. D. K. Yang and S. T. Wu, *Fundamentals of Liquid Crystal Devices* (John Wiley and Sons, 2014).
33. T.-H. Yoon, K. H. Kim, D. H. Song, and J. C. Kim, "Fast switching technologies for a nematic liquid crystal cell," *Proc. SPIE* **7956**, 79560M (2011).
34. D. Xu, H. Chen, S. T. Wu, M. C. Li, S. L. Lee, and W. C. Tsai, "A fringe field switching liquid crystal display with fast grayscale response time," *J. Disp. Technol.* **11**(4), 353–359 (2015).
35. H. Chen, Z. Luo, D. Xu, F. Peng, S. T. Wu, M. C. Li, S. L. Lee, and W. C. Tsai, "A fast-response A-film-enhanced fringe field switching liquid crystal display," *Liq. Cryst.* **42**(4), 537–542 (2015).
36. D. H. You, C. J. Yu, and S. D. Lee, "Reflective configuration of vertically aligned deformed-helix ferroelectric liquid crystal display," *Ferroelectrics* **278**(1), 233–240 (2002).
37. H. Kikuchi, M. Yokota, Y. Hisakado, H. Yang, and T. Kajiyama, "Polymer-stabilized liquid crystal blue phases," *Nat. Mater.* **1**(1), 64–68 (2002).
38. K. M. Chen, S. Gauza, H. Xianyu, and S. T. Wu, "Submillisecond gray-level response time of a polymer-stabilized liquid crystal," *J. Disp. Technol.* **6**(2), 49–51 (2010).
39. J. Kim, C. Oh, M. J. Escuti, and S. Serati, "Wide-angle nonmechanical beam steering using thin liquid crystal polarization gratings," *Proc. SPIE* **7093**, 709302 (2008).
40. K. M. Johnson, D. J. McKnight, and I. Underwood, "Smart spatial light modulators using liquid crystals on silicon," *IEEE J. Quantum Electron.* **29**(2), 699–714 (1993).
41. H. Dai, K. Xu, Y. Liu, X. Wang, and J. Liu, "Characteristics of LCoS phase-only spatial light modulator and its applications," *Opt. Commun.* **238**(4-6), 269–276 (2004).
42. D. Dudley, W. M. Duncan, and J. Slaughter, "Emerging digital micromirror device (DMD) applications," *Proc. SPIE* **4985**, 14–25 (2003).
43. J. Li, C. H. Wen, S. Gauza, R. Lu, and S. T. Wu, "Refractive indices of liquid crystals for display applications," *J. Disp. Technol.* **1**(1), 51–61 (2005).
44. ITU-R Recommendation BT.2020, "Parameter values for ultra-high definition television systems for production and international programme exchange," 2012.
45. K. Masaoka, Y. Nishida, M. Sugawara, and E. Nakasu, "Design of primaries for a wide-gamut television colorimetry," *IEEE Trans. Broadcast* **56**(4), 452–457 (2010).
46. R. Zhu, Z. Luo, H. Chen, Y. Dong, and S. T. Wu, "Realizing Rec. 2020 color gamut with quantum dot displays," *Opt. Express* **23**(18), 23680–23693 (2015).

47. E. Jang, S. Jun, H. Jang, J. Lim, B. Kim, and Y. Kim, "White-light-emitting diodes with quantum dot color converters for display backlights," *Adv. Mater.* **22**(28), 3076–3080 (2010).
48. Z. Luo, Y. Chen, and S. T. Wu, "Wide color gamut LCD with a quantum dot backlight," *Opt. Express* **21**(22), 26269–26284 (2013).
49. C. H. Chen, F. C. Lin, Y. T. Hsu, Y. P. Huang, and H. P. D. Shieh, "A field sequential color LCD based on color fields arrangement for color breakup and flicker reduction," *J. Disp. Technol.* **5**(1), 34–39 (2009).

1. Introduction

Immersive virtual reality and augmented reality (VR/AR) are two emerging wearable display technologies [1–4] with potential applications for entertainment, education, training, design, advertisement, and medical diagnostics. One of the key challenges of these head-mounted displays is to track eyeball movement [5–7]. With that, the displayed images could be steered into human eyes dynamically, otherwise the images would be lost if the eyeballs move away from the sweet spot. Therefore, an efficient beam steering device is highly desirable to ensure good viewing experience regardless of the eyeball movement. Different from conventional laser beam steering [8–11], the VR/AR display systems demand red, green, and blue colors, high optical efficiency, fast response time, low power consumption, lightweight, compact packaging, and low cost.

Recently, a new beam steering device using cycloidal diffractive waveplate (CDW) has been demonstrated [12–16]. It offers a potential solution for eye tracking of the VR/AR systems. The CDW consists of a thin liquid crystal (LC) layer, wherein the LC optical axis rotates continually along a Cartesian axis. A unique feature of CDW is its high diffraction efficiency (> 95%) for a circularly polarized beam. If the incident light is linearly polarized, then both + 1st and –1st diffraction orders would appear. Previous efforts were mainly focused on steering a laser beam [13, 17], yet little attention was paid on steering red (R), green (G), and blue (B) colored images for display applications. The major challenge for steering RGB beams is color dispersion, i.e. different color exhibits a different diffraction angle.

In this paper, we demonstrate a switchable beam steering device with CDW for VR/AR applications. A systematic study is conducted from the device working mechanism to the potential problems and their corresponding solutions. In Sec. 2, we build a rigorous model to simulate the performance of CDW with commercial software COMSOL. Next, in Sec. 3 we propose a simple device to switch the input polarization between right-handed circular polarization (RCP) and left-handed circular polarization (LCP). Such a polarization switch consists of a twisted nematic (TN) LC cell and an achromatic quarter-wave ($\lambda/4$) plate. A typical response time of a TN cell is around 10 ms. If we use a thin TN cell, then the response time can be reduced to submillisecond. Finally in Sec. 4, we discuss the color dispersion effect of CDWs. High efficiency (>90%) is obtained over a wide range of wavelengths by choosing a proper LC material, and two approaches are proposed to mitigate the dispersion issue and achieve the same diffraction angles for RGB lights for display applications.

2. Modeling of CDW

To investigate the underlying operation mechanism, firstly we built a rigorous model using commercial finite element package, called COMSOL Multiphysics. The LC director distribution in a CDW is varying continually with spatial modulation period Λ as Fig. 1 depicts:

$$\vec{n} = \{\cos(qx), \sin(qx), 0\}, q = 2\pi / \Lambda. \quad (1)$$

The physical properties of this structure are modulated with period $\Lambda/2$ due to the physical equivalence of the $+\vec{n}$ and $-\vec{n}$ directions of the LC directors. We assume the CDW thickness L and LC birefringence Δn satisfy the half-wave phase retardation condition, i.e. $L\Delta n = \lambda/2$. Next, we performed simulations with following steps: designing device geometry,

selecting materials, setting initial and boundary conditions, and defining finite element mesh. All the formulations are based on Maxwell equations together with boundary conditions; while previous simulations were typically conducted using Jones matrix approach [16, 18] and conventional grating theory to evaluate the final CDW performance, e.g. diffraction angle and diffraction efficiency. Although these analytical solutions give physical insights and work reasonably well in some aspects, some new phenomena are obscured, e.g. the peak diffraction efficiency does not occur at normal incidence angle, and instead it deviates by 8° .

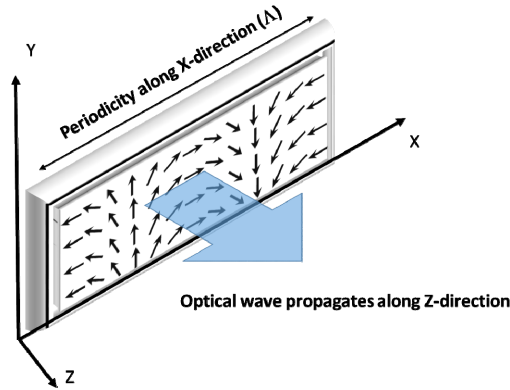


Fig. 1. Schematic structure of the cycloidal diffractive waveplate.

To validate our simulation, in experiment we prepared a cycloidal diffractive waveplate. The detailed fabrication procedures have been described in [14, 16]. Briefly speaking, two coherent laser beams of orthogonal circular polarization overlap on the substrate carrying the photoalignment layer. In the overlapped region, the effective polarization of such beams is linear and rotating in a cycloidal manner. As a result, the LC directors are oriented successfully by the photoalignment pattern. In our experiment, the employed LC Δn is 0.15, and thickness is controlled at $L = 2.11 \mu\text{m}$ to satisfy the half-wave condition at $\lambda = 633 \text{ nm}$. Another important parameter is spatial period $\Lambda = 4.88 \mu\text{m}$. We input these parameters to our model and simulated the device performance.

Figures 2(a) and 2(b) show the calculated deflection angles for right-handed circularly polarized light and linearly polarized incident light, respectively. Clearly, the circular polarization dependency is validated for CDW as only one diffraction order (+1st) exists for the incident RCP light and two diffraction orders (+1st and -1st) appear if the incident light is linearly polarized. Also, the simulated diffraction angle $\theta = 15.0^\circ$ is very close to the measured one $\theta = 15.5^\circ$. Meanwhile, the obtained diffraction efficiency for RCP is 97.3%, which agrees well with the measured result 95.2%.

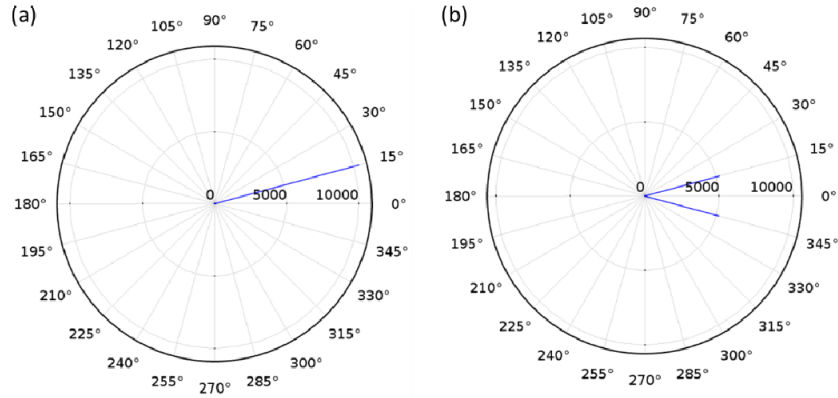


Fig. 2. Simulated diffraction angles for (a) right-handed circularly polarized incident light, and (b) linearly polarized incident light.

Next, we investigate the wavelength dispersion effect of CDWs. The simulation and experimental results are depicted in Fig. 3. The black curve represents our calculated diffraction efficiency (η) using COMSOL program, while the blue curve shows the result using following simplified equation based on Jones matrix approach [16, 18]:

$$\eta(\lambda) = \sin^2 \frac{\pi L \Delta n}{\lambda}. \quad (2)$$

Both simulation results agree with experimental data (red dots) reasonably well. As the wavelength deviates from the optimized value (here it is $\lambda = 633$ nm), the half-wave condition is no longer satisfied so that the corresponding efficiency decreases. From Fig. 3, when the wavelength decreases from 633 nm to 457nm, the diffraction efficiency declines rapidly from 95.2% to 21.0%. For VR/AR displays using red, green and blue light sources, such dispersion effect is severe and a better design is needed. An example for reducing the color dispersion effect will be given in Sec. 4.

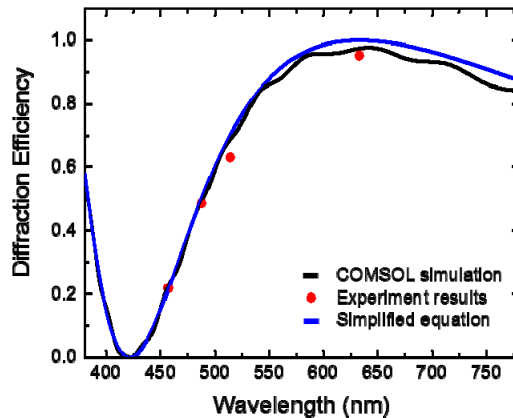


Fig. 3. Dispersion effect of cycloidal diffractive waveplate.

As the incident angle changes, the diffraction angle (θ) will change accordingly. An excellent match between the measured results and simulation results is plotted in Fig. 4. From Fig. 4(a), when the incident angle is within $\pm 30^\circ$, the diffraction angle is roughly linear to the incident angle. If we consider the relative diffraction angle, defined as $\theta_{relative} = |\theta_{diffraction} -$

$\theta_{incident}$), shown in Fig. 4(b), within the $\pm 20^\circ$ incident angle range the relative diffraction angle is kept at 15° with a small deviation of $\sim 2^\circ$.

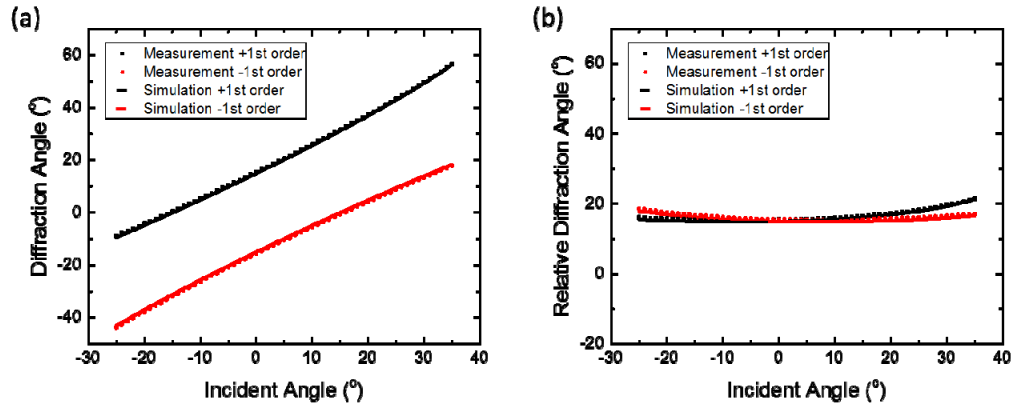


Fig. 4. Incident angle dependent (a) diffraction angle, and (b) relative diffraction angle.

As the incident angle deviates from its optimum, diffraction efficiency for a laser beam of 633 nm wavelength declines gradually, as Fig. 5(a) depicts. But interestingly, the highest efficiency doesn't occur at normal incidence; rather it occurs at $\theta \approx 8^\circ$. This is verified by both experiment and simulation. The reason is believed to originate from the deviated effective optical path inside the CDW. The thickness L of CDW is designed to satisfy the half-wave condition ($L\Delta n = \lambda/2$) and is considered as the optical length thereafter. But in reality the optical path inside the CDW is not a straight line, as illustrated clearly in Fig. 5(b). Therefore, the effective optical length L_{eff} will be different from the original one, leading to the 8° shift from normal for the highest efficiency to occur. With our rigorous model, this phenomenon is fairly easy to understand, but for the simplified model described in Eq. (2) the underlying physical mechanism is obscured. Therefore, our model is a powerful tool to optimize the CDW design and performance.

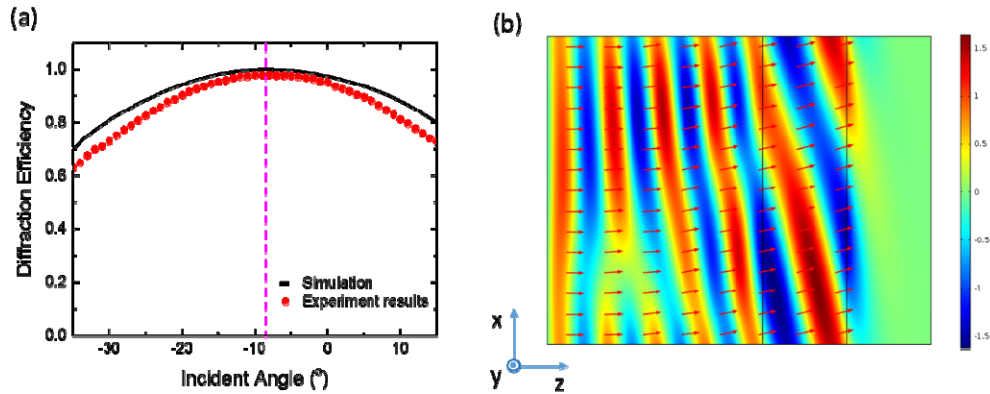


Fig. 5. (a) Relationship between diffraction efficiency and incident angle, and (b) Simulated field distributions within one spatial period structure using COMSOL Multiphysics. The axes coincide with the schematic diagram in Fig. 1, where the horizontal axis (z) is the light propagation direction, and vertical axis (x) is periodic structure of CDW; Red arrows represent the power flow or Poynting vector.

3. Polarization switch

In principle, there are two types of CDW-based beam steering devices: active and passive [16]. For active devices, the CDW is made of LC material and can be tuned by the applied voltage. For example, in the voltage-off state, it works as a diffractive waveplate (i.e. +1st or -1st order depending on the input circular polarization); while in the voltage-on state the LC directors are reoriented along the electric field direction and the diffraction effect disappears. As a result, the beam passes through the CDW directly (i.e. 0th order). Therefore, such an active CDW is switchable between +1st order (or -1st order) and 0th order. But it requires two substrates over-coated with indium tin oxide (ITO) electrodes, leading to increased bulkiness, heavier weight, and lower transmittance. Moreover, to make it switchable between +1st order and -1st order, an external polarization switch is still needed.

On the other hand, a passive CDW is made of LC polymeric film and is not switchable. Thus, an additional polarization switch is required to select the +1st or -1st order. A passive CDW is thin (several microns), lightweight, and highly transmissive. But to get 0th order (non-diffraction), several CDWs have to be placed in sequence [19], as will be discussed later.

In our experiment, we used a passive CDW to illustrate the working principles. For the convenience of discussion, let us assume in the VR/AR system the incident image is linearly polarized from a liquid crystal display (LCD) panel. Then the CDW would diffract the incident linearly polarized light to +1st order and -1st order with equal intensity, as Fig. 2(b) shows. Thus, we need an electro-optic device to first convert the input linearly polarized light to circular, and then switch the polarization between RCP and LCP.

For a laser beam, we can use a homogeneous (HG) cell or a vertical-alignment (VA) cell to switch between RCP and LCP [17, 20]. However, for a broadband light source, HG and VA cells are not usable because of their strong wavelength dispersion effect. The input RCP will not be converted to LCP completely, which would degrade the final performance greatly. To solve this issue, here we propose to use a 90° twisted nematic (TN) cell with an achromatic quarter-wave ($\lambda/4$) film, as Fig. 6 shows. TN is an electrically tunable achromatic half-wave ($\lambda/2$) plate and has been widely used as a polarization switch for adaptive lens [21–23]. Different from HG and VA cells, TN in combination with a quarter waveplate is able to convert the input RCP into LCP perfectly due to the polarization rotation effect [21], which is highly desirable for VR/AR display applications.

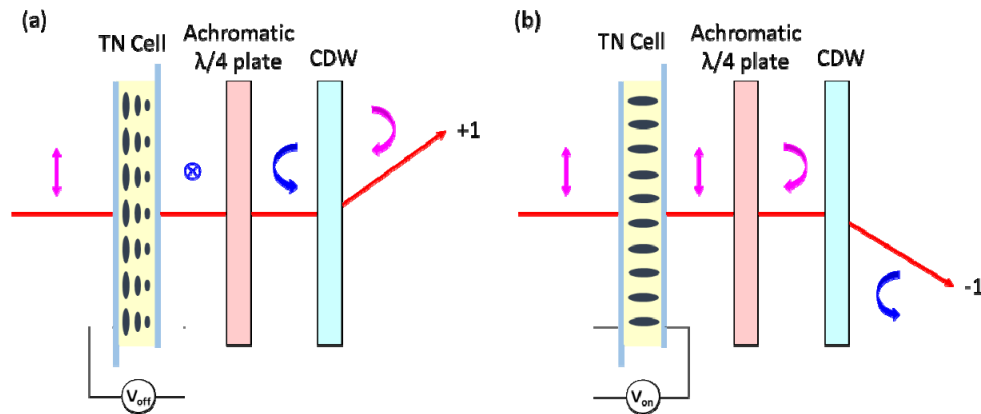


Fig. 6. Schematic diagram of proposed optical switch based on CDW.

As shown in Fig. 6, the input light from an LCD is linearly polarized, say p-wave. At the voltage-off state ($V_{off} = 0$), the output light after TN cell is converted to s-wave due to the polarization rotation effect. After passing through the achromatic $\lambda/4$ plate, it becomes

circularly polarized, say RCP, which will be deflected to +1st order by CDW [Fig. 6(a)]. In a high voltage state ($V_{on} \sim 5V$), the LC directors of the TN cell are reoriented along the electric field direction so that the polarization rotation effect vanishes. The input p-wave remains unchanged after the TN cell and then becomes LCP after traversing through the $\lambda/4$ plate. As a result, the beam is deflected to the -1st order [Fig. 6(b)]. In this case, a simple optical switch between +1st and -1st diffraction orders can be achieved by controlling the applied voltage.

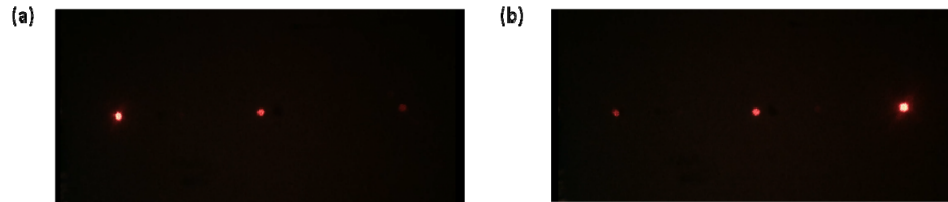


Fig. 7. Captured images at (a) voltage-off state and (b) voltage-on state.

To prove the concept, in experiment we prepared a TN cell using ITO (indium tin oxide) glass substrates. The cell gap was controlled at $d = 5.0 \mu\text{m}$ with spacer balls. The physical properties of the employed LC mixture are listed as follows: $\Delta n = 0.109 @ \lambda = 633 \text{ nm}$, $\Delta \varepsilon = 9.5$, rotational viscosity $\gamma_1 = 57.0 \text{ mPas}$ and splay elastic constant $k_{11} = 11.5 \text{ pN}$. A He-Ne laser was used as probing beam and the diffracted power was detected by a New Focus large-area visible photoreceiver (Model 2031). The captured images of the voltage-off and -on states are shown in Fig. 7(a) and 7(b), respectively. As expected, the diffraction order switches from +1st order to -1st order or vice versa. From the photos, all three diffraction orders (i.e. -1st order, 0th order, and +1st order) are visible, but through measurements the major power ($> 95\%$) lies in the primary diffraction order. The efficiency of 0th order is about 4.6%, while other orders occupy less than 0.2%. The obtained contrast ratio of the primary diffraction order is $\sim 500:1$.

We also measured the response time at $V_{on} = 5 \text{ V}$, and results are depicted in Fig. 8. The rise time is 10.8 ms and decay time is 1.8 ms. To improve response time, we could use a thinner TN cell filled with a higher Δn yet low viscosity LC mixture [24–26] and apply overdrive and undershoot voltages [27, 28]. By using a 1.6- μm cell gap, sub-millisecond response time can be achieved [29]. Another approach is to use a dual-frequency liquid crystal (DFLC) mixture [30]. The advantage of DFLC is both fast rise time and decay time can be achieved, but the tradeoff is increased voltage. As for the practical applications, 120 Hz sampling frequency is typically employed for eye tracking in head-mounted displays [31]. Therefore, our devices are fast enough for the current display technology. On the other hand, the response time of liquid crystal display (LCD) has been improved to be less than 5 ms [32]. With some device structure optimization [33–35] or new LC mode [36–38], faster response time can be achieved.

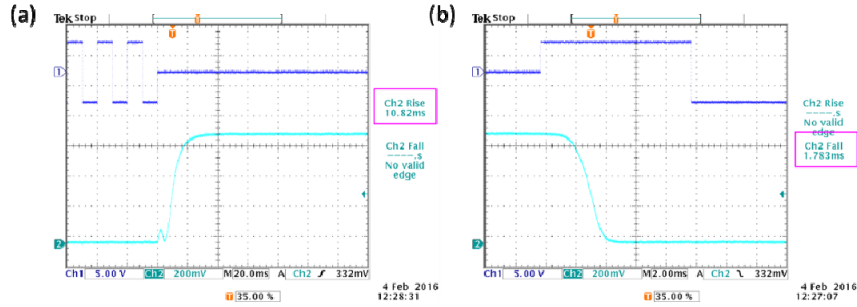


Fig. 8. Measured response time of the optical switch: (a) rise time, and (b) decay time.

4. Results and discussion

4.1 Multiple diffraction angles

In Sec. 3, we only show the switch between +1st order and -1st order, but for eye tracking in a VR/AR system we need multiple diffraction angles. In this case, cascaded CDW design should be considered [39], as shown in Fig. 9.

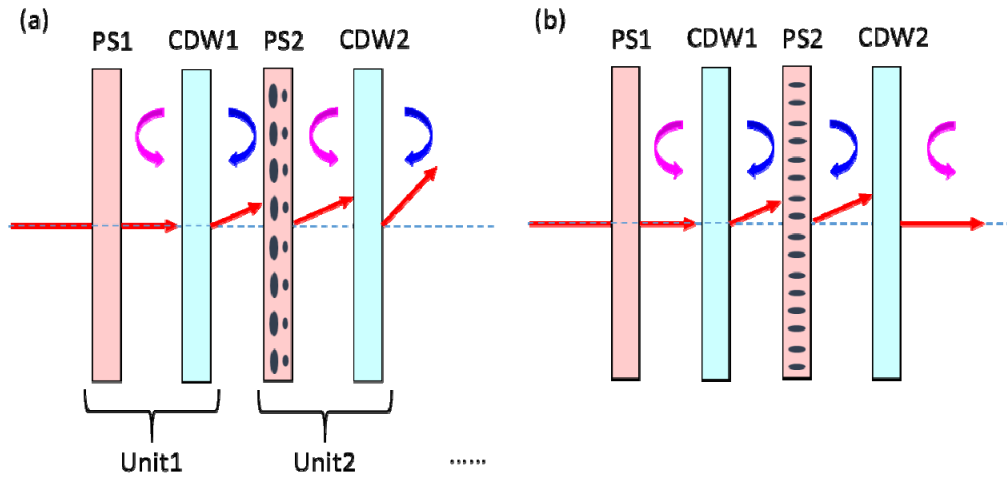


Fig. 9. Cascaded design using multiple CDWs in sequence. PS: polarization switch; CDW: cycloidal diffractive waveplate.

Each unit of the cascaded design is composed of a polarization switch (PS: TN cell with an achromatic $\lambda/4$ plate) and a CDW. The working mechanism is the same as discussed above, but the final diffraction angle will be determined by the combination of each CDW. Let us assume the diffraction angle of each CDW is θ_1 , θ_2 , and θ_3 . Then by simple arithmetic, all possible diffraction angles are listed in Fig. 10. Using this chart, each CDW would be specified easily for different requirements. For example, if the required diffraction angles are 0° , $\pm 5^\circ$, $\pm 10^\circ$, and $\pm 15^\circ$, then according to Fig. 10, the diffraction angles of each CDW should be $\theta_1 = 7.5^\circ$, $\theta_2 = 2.5^\circ$, and $\theta_3 = 5^\circ$. If more CDWs are cascaded, more diffraction angles can be obtained [39]. Other beam steering technologies can also achieve the same performance, like spatial light modulator using liquid-crystal-on-silicon (LCoS) [40, 41] or digital micro-mirror device (DMD) [42]. However, both LCoS and DMD are reflective devices, which means the required optical design is more complicated and the whole system would be bulky. Our CDW-based device is transmission type; therefore, the optical design is fairly straightforward, which makes the AR/VR system compact and lightweight.

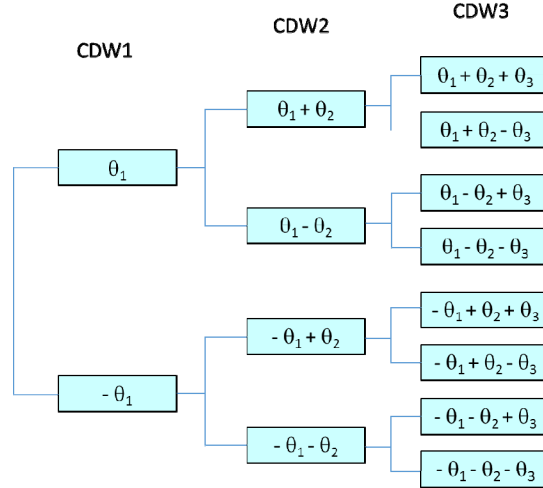


Fig. 10. Possible diffraction angles for three cascaded CDWs.

4.2 Broadband operation

For free-space optical communications, a laser is commonly used and our CDW works well. To enable CDW for broadband operation, such as VR/AR system, the peak wavelength has to be chosen carefully. In our design, CDW is optimized at $\lambda = 532$ nm and an LC mixture with a relatively small refractive index dispersion is employed. Typically, the refractive indices of LC materials can be described by the three-band model [43]:

$$n_e = A_e + \frac{B_e}{\lambda^2} + \frac{C_e}{\lambda^4}, \quad (3)$$

$$n_o = A_o + \frac{B_o}{\lambda^2} + \frac{C_o}{\lambda^4}, \quad (4)$$

where n_e and n_o represent the extraordinary and ordinary refractive indices, and $A_{e,o}$, $B_{e,o}$ and $C_{e,o}$ are the corresponding Cauchy coefficients. Here we chose Merck LC mixture MLC-9200-000 as an example to reduce the dispersion effect. The Cauchy coefficients are summarized as: $A_e = 1.5382$, $B_e = 0.0073$, $C_e = 4.00\text{e-}5$, $A_o = 1.4600$, $B_o = 0.0058$, and $C_o = 3.95\text{e-}17$. The half-wave condition is calculated for $\lambda = 532$ nm, and the resultant thickness is $L = 3.17$ μm .

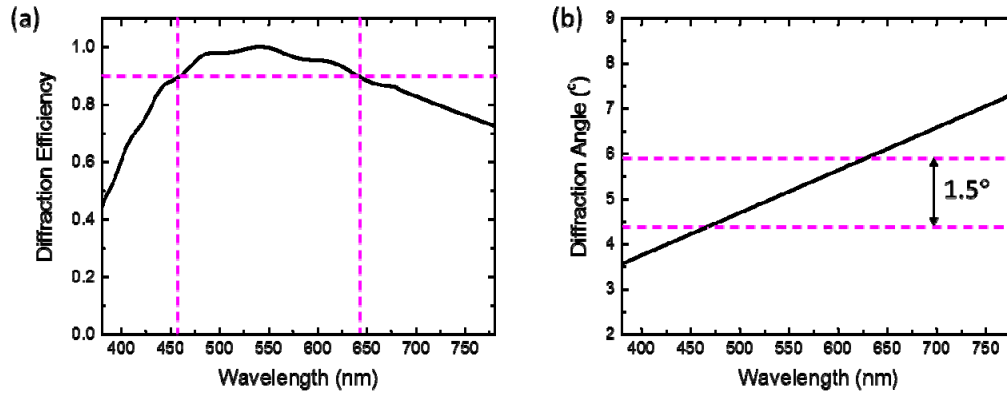


Fig. 11. (a) Simulated wavelength dependent diffraction efficiency, and (b) wavelength dependent diffraction angle.

Figure 11(a) shows the simulated wavelength-dependent diffraction efficiency. When the wavelength changes from 460 nm to 640 nm, diffraction efficiency keeps over 90%, which is desirable for real applications. Also, for quantum dot-enhanced LCD backlight, the optimized RGB wavelengths for Rec. 2020 color gamut is 630 nm, 532 nm, and 467 nm, respectively [44–46]. The obtained working band (460 nm ~640 nm) could be incorporated with such backlight easily to get high optical efficiency and wide color gamut [47, 48].

The biggest challenge of CDW for full-color displays using white LED or RGB light source is wavelength dependent diffraction angle. As Fig. 11(b) shows, the diffraction angle increases with the wavelength. Here, the diffraction angle for 532 nm is set at 5°, while for 467 nm (blue) and 630 nm (red) the diffraction angle becomes 4.4° and 5.9°, respectively. The variation is 1.5°, which leads to undesirable rainbow pattern at the edge of displayed image. Presently, we do not have a simple solution to correct the dispersion for the white LED light source. But if the light source is RGB LEDs, then the following two approaches would help mitigate the color dispersion effect.

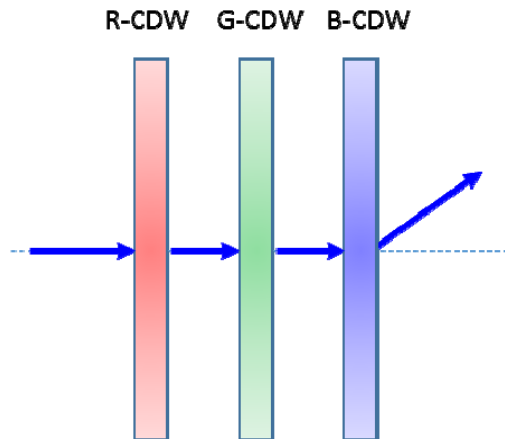


Fig. 12. Schematic diagram of proposed optical switch with three independent parts: red (R), green (G), and blue (B) CDWs.

Let us first discuss the field-sequential color displays [24, 49], in which the RGB LEDs blink at different time sequence, and its frame rate is synchronized with that of CDWs, as Fig. 12 shows. The wavelength dependent diffraction angle can be approximated by the simple grating equation as:

$$\theta(\lambda) \approx \sin^{-1}(\lambda / \Lambda). \quad (5)$$

From Eq. (5), if we optimize each CDW by keeping the same λ/Λ ratio for each color, then the diffraction angle would remain the same for the RGB wavelengths. Let us illustrate the working principles using the example shown in Fig. 12. In the sub-frame that only blue LED is on, while the red and green CDWs are off (i.e. their diffraction angle is 0°), then only the blue CDW deflects the incident blue light. Similarly, we can synchronize the CDWs with LEDs and steer the RGB beams to the same angle. To enable 0° diffraction angle (i.e. 0th order), we can simply a voltage to the active CDW, while for passive CDW we need cascaded design as Fig. 10 shows.

The second possible solution is to slightly tilt the individual incident angle of the RGB LEDs. From Fig. 11(b), we need to reduce the diffraction angle by $\sim 0.9^\circ$ for red light, while increasing the diffraction angle by $\sim 0.6^\circ$ for blue. Under such a circumstance, we can use a single CDW (instead of three CDWs) to steer the RGB colors. Undoubtedly, the complexity of the illumination (or optical) system would increase. As discussed above, the diffraction efficiency declines gradually as the incident angle deviates from its optimal value. Figure 13 shows the simulated incident angle dependent diffraction efficiency of our passive CDW unit at $\lambda = 532$ nm. It has a relatively wide acceptance angle. For such a small incident angle variation ($< 1.5^\circ$) the diffraction efficiency for RGB remains basically the same.

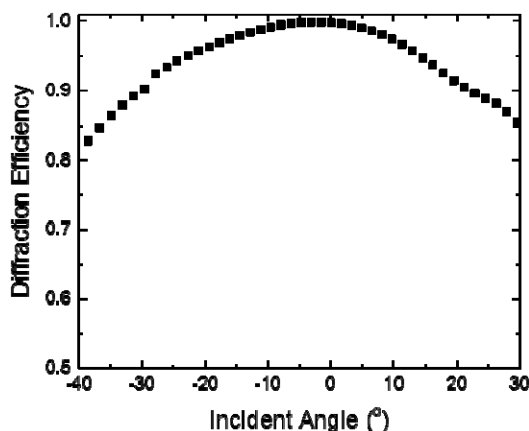


Fig. 13. Simulated incident angle dependent diffraction efficiency at $\lambda = 532$ nm.

5. Conclusion

We have proposed to use cycloidal diffractive waveplates in a VR/AR system to dynamically deflect the output images to human eye. The key part is a TN cell working as a switchable achromatic half-wave plate along with an achromatic quarter-wave plate. By controlling the applied voltage to TN cell, the diffracted light can be rapidly switched from + 1st order to -1st order or vice versa. Also, by cascading 2-3 CDWs in sequence, multiple diffraction angles can be achieved. Meanwhile, high efficiency is obtained within a broadband of wavelengths and wide incidence angles. To solve the dispersion issue, two approaches were proposed to obtain the same diffraction angle if the light source is RGB LEDs. This design exhibits several advantages including high optical efficiency, fast response time, low power consumption, compact and lightweight packaging. It holds great potential for virtual reality and augmented reality display applications.

Acknowledgments

The authors would like to thank Guanjun Tan for helpful discussions, and AFOSR for partial financial support under contract No. FA9550-14-1-0279.